nature photonics

Article

https://doi.org/10.1038/s41566-024-01548-2

Near-petahertz fieldoscopy of liquid

Received: 31 October 2023

Accepted: 14 September 2024

Published online: 21 October 2024

Check for updates

Anchit Srivastava[1,2], Andreas Herbst[1,2], Mahdi M. Bidhendi[1,2], Max Kieker[1,2], Francesco Tani[1,3] & Hanieh Fattahi[1,2]

Measuring transient optical fields is pivotal not only for understanding ultrafast phenomena but also for the quantitative detection of various molecular species in a sample. Here we demonstrate near-petahertz electric field detection of a few femtosecond pulses with 200 attosecond temporal resolution and subfemtojoule detection sensitivity. By field-resolved detection of the impulsively excited molecules in the liquid phase, termed femtosecond fieldoscopy, we demonstrate temporal isolation of the response of the target molecules from those of the environment and the excitation pulse. In a proof-of-concept analysis of aqueous and liquid samples, we demonstrate field-sensitive detection of combination bands of 4.13 μmol ethanol for the first time. This method expands the scope of aqueous sample analysis to higher detection sensitivity and dynamic range, while the simultaneous direct measurements of phase and intensity information pave the path towards high-resolution biological spectro-microscopy.

Laser-based, label-free quantitative determination of sample composition has proven to be a potent tool across a wide spectrum from fundamental research to real-life applications[1–11]. For accurate and delicate spectroscopic measurements, it has been crucial to isolate the sample from environmental interferences. For instance, water accounts for approximately 60% of the human body, envelops 70% of the Earth's surface and permeates our surroundings through the atmosphere. Water has a broad absorption spectrum spanning from the visible to mid-infrared (MIR) and is a persistent component on our detectors. Due to its strong absorption cross-section at MIR, sensitive spectroscopy of samples at their resonance frequencies is challenging, as water dominates other, more subtle, absorbance features arising from other molecules. Moreover, the excessive absorbed energy by water at MIR is left in the sample as thermal energy, limiting non-invasive analysis. Meanwhile, near-infrared (NIR) spectroscopy provides a fingerprint of sample constituents similar to MIR spectroscopy. It distinguishes itself by offering higher spatial resolution and enhanced penetration depth, afforded by the lower absorption cross-section of water in the NIR region[12–14]. This feature makes NIR spectroscopy particularly suitable for the non-invasive and label-free examination of soft matter and large-volume aqueous samples[15,16].

Overtone and combination vibrations of molecules, which are primarily detected in NIR spectroscopy, extend beyond 0.12 PHz. Spectrometers have been used for frequency domain detection in this range. However, their detection sensitivity is constrained by the excitation light, which manifests as a background within the same spectral range[17–19]. Since the resonance frequencies of overtone and combination bands surpass the sensitivity of silicon-based detectors, employing a second detector, generally more prone to noise in this range, is necessary to capture the system's entire response. Fourier transform spectroscopy is an alternative method allowing for precise spectroscopic detection. Recent advancements in NIR dual-comb spectroscopy have paved the way for precision Fourier transform spectroscopy, albeit primarily in the gas phase[20–24]. Nonetheless, the technique remains constrained by detectors' spectral response and the existence of a background signal analogous to frequency domain detection[13,25].

In contrast, field-resolved detection allows the direct measurement of light–matter interactions with attosecond precision in a sub-cycle regime, capturing both amplitude and phase information[26,27]. For decades, attosecond streaking was the sole method to probe the electric field of light with a bandwidth approaching the petahertz range[28,29]. A significant drawback was its confinement to vacuum operations. Over the past decade, various techniques have been developed that enable the near-petahertz field-resolved detection of light in ambient air[30–46]. Among these techniques, electro-optic sampling (EOS) stands

[1]Max Planck Institute for the Science of Light, Erlangen, Germany. [2]Friedrich-Alexander-Universität Erlangen–Nürnberg, Erlangen, Germany. [3]PhLAM – Physique des Lasers Atomes et Molécules, Université Lille, CNRS, UMR 8523, Lille, France. e-mail: hanieh.fattahi@mpl.mpg.de

https://doi.org/10.1038/s41566-024-01548-2

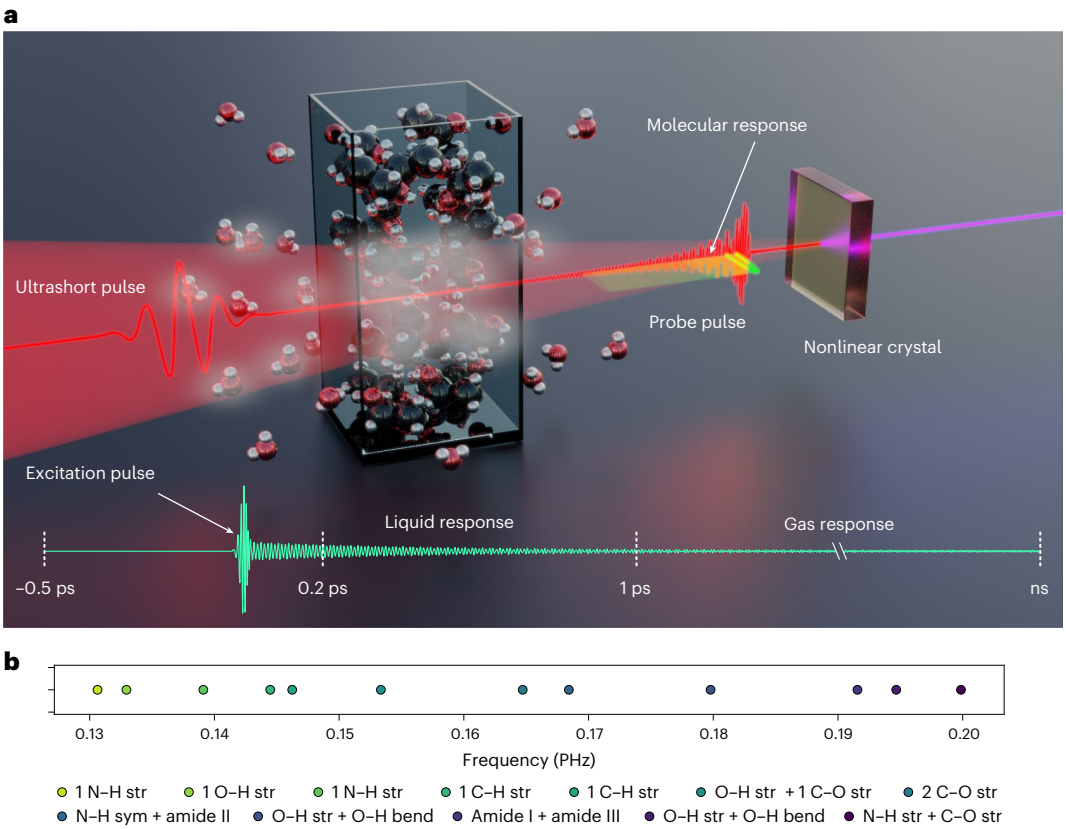

Fig. 1 | Near-petahertz fieldoscopy. a, An ultrashort pulse excites molecules at their NIR resonances. Here, the molecules inside a cuvette represent the sample under scrutiny, while the surrounding molecules represent atmospheric water vapour molecules. The transmitted field accumulates dispersion during propagation and contains the global molecular response of both the sample and the environment. A second short pulse at higher frequencies is used for up-conversion and generation of a delay-dependent signal in a nonlinear crystal, where the correlation signal is directly proportional to the electric field of the excitation pulse. The measured electric contains the ultrashort excitation pulse, the delayed response of the liquid spanning over several picoseconds, and a long-lasting response of atmospheric gases lasting for hundreds of nanoseconds. By time filtering and subsequent data analysis, the molecular response can be decomposed to the short-lived liquid and long-lived gas responses. **b**, The biologically relevant vibrational modes at NIR spectral range. Different compounds, including proteins, carbohydrates, lipids, polyphenols and alcohols, are associated with the shown bands. Associated bonds are described in the legend below the plot, where 'str' refers to stretching vibration and 'bend' refers to bending vibration. The numbers 1 and 2 indicate the first and second overtones, while the plus sign (+) indicates combination bands. The values were taken from ref. 16. The liquid and gas responses shown in the figure are enhanced for better visibility.

out for its unparalleled detection sensitivity[27,47,48]. In EOS, a short probe pulse is employed to resolve the cycles of the electric field of light by up-converting its spectral bandwidth to higher frequencies, making it possible to apply silicon detectors for broadband NIR detection[49]. Moreover, the combination of bright ultrashort pulses[50–53] and heterodyne detection allows higher detection signal-to-noise ratio and higher detection sensitivity, leaving the shot noise of the probe pulse the primary source of noise[54].

In this work, we report on the direct detection of the electric field of light at near-petahertz frequencies. This has been enabled by developing a unique laser source delivering broadband pulses with carrier-to-envelope phase (CEP) stability, which were intrinsically synchronized to near-single-cycle pulses at megahertz repetition rates. The unique frontend enabled direct electric-field detection of CEP-stable few-cycle pulses with high detection sensitivity and dynamic range via EOS with attosecond temporal resolution.

Employing the bright ultrashort pulses, we report on the field-sensitive detection of molecular response at the NIR region. Few-femtosecond phase-coherent pulses were utilized for both broadband molecular excitation and the near-petahertz electric-field detection of their response. Here, the confinement of the excitation pulses allows temporal gating of the molecular response, while accessing the electric field enables the precise detection of the response of the target molecules from those of the environment. We evaluated our approach by conducting field-resolved detection of water vibration modes in both gas and liquid phases in the NIR region. In addition, we detected the subtle combination bands of ethanol in the liquid phase. These results show a field detection of the NIR molecular response in ambient air, paving the path for the emergence of innovative, field-sensitive, label-free spectroscopy and microscopy techniques.

Results

Figure 1 illustrates the measurement concept. Few-cycle CEP-stable NIR pulses, are utilized to extract sensitive spectroscopic information from liquid samples under atmospheric conditions. The electric field of the molecular response, in the wake of the excitation pulse, is resolved via EOS. Due to the high detection sensitivity, we can resolve not only the response of the molecular vibrations of the sample at their overtone and combination resonances but also the response of atmospheric molecules along the beam path. The temporal confinement of the excitation pulses ensures that the molecular responses from both the sample and ambient air are temporally separated from the excitation pulse. Moreover, the response of the liquid sample is temporally distinguished from the ambient air's fingerprint owing to the faster dephasing in the liquid phase. Realizing such a concept

https://doi.org/10.1038/s41566-024-01548-2

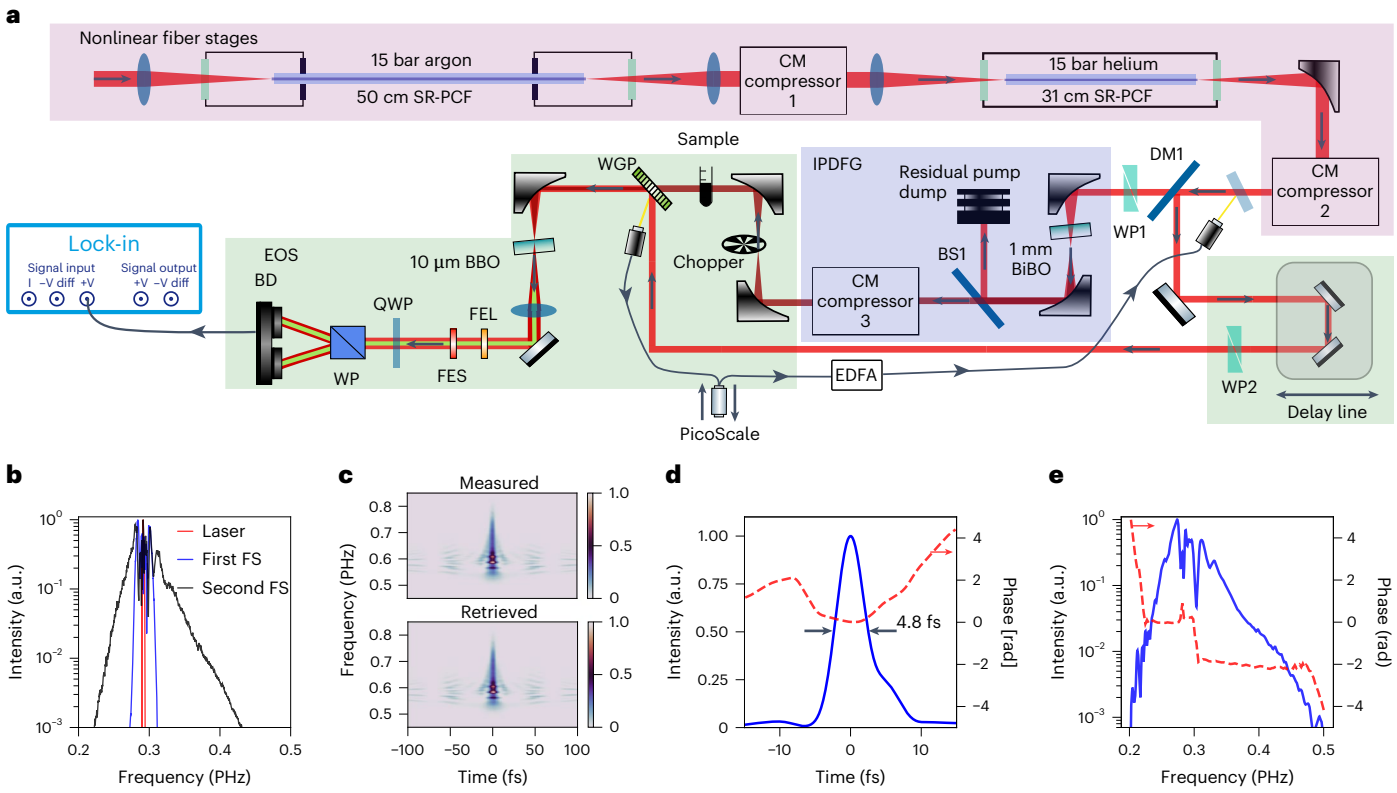

Fig. 2 | Experimental setup. a, The shaded regions highlight different parts of the optical setup: nonlinear fibre stages in pink, IPDFG in blue and EOS in green. **b**, The spectrum of the laser (red), the first fibre stage (blue) and the second fibre stage black). **c**, Measured (top) and retrieved (bottom) spectrograms. The near-single-cycle pulses were measured after the nonlinear compression stages via SHG-FROG. **d**, The retrieved temporal pulse duration at the output of the second fibre at a 1 MHz repetition rate. **e**, The retrieved spectral intensity and phase. DM, dichroic mirror; WP, wedge pair; BS, beam splitter; WGP, wire grid polarizer; FEL, long-pass filter; FES, short-pass filter; QWP, quarter-wave plate; BD, balanced photodiode; EDFA, erbium-doped fibre amplifier; FS, fiber stage.

requires the generation of intrinsically synchronized bright few-cycle pulses with at least one-octave separation and subcycle temporal synchronization.

The pink-shaded region in Fig. 2a shows the optical setup for near-single-cycle pulse generation at megahertz repetition rates. Single-ring hollow-core photonic crystal fibres (SR-PCF) are used due to their relatively low-loss broadband guidance and tunable dispersion[55,56], allowing the generation of ultrashort, bright pulses containing tens of microjoules of energy[53,57]. In the first stage, 20 µJ, 1 MHz laser pulses were compressed from 255 fs to 25 fs at full width at half maximum (FWHM), by self-phase-modulation-based spectral broadening in argon-filled SR-PCF (Supplementary Figs. 1 and 2), followed by group-delay dispersion compensation by a chirped mirror (CM) compressor. Subsequently, in the second stage, the 25 fs pulses were compressed to a near-single-cycle duration via soliton-effect self-compression in a similar fibre (Fig. 2b). In both stages, the gas species used as a medium were selected to minimize photoionization and subsequent long-lived effects occurring at megahertz repetition rates[58]. The accumulated dispersion on the near-single-cycle pulses owing to propagation in media after the fibre was compensated in a CM compressor to 4.8 fs at FWHM, limited by the bandwidth of the CM compressor (Fig. 2c,d and Supplementary Fig. 3). This corresponds to 3.5 GW of peak power with 69% of the energy in the main pulse. The retrieved spectrum shown in Fig. 2e spans over 300 THz bandwidth supporting 3 fs pulses at FWHM.

Intrapulse difference frequency generation (IPDFG) was employed to generate broadband NIR pulses with a passive CEP stability (Fig. 2a, blue region)[59]. A 500-µm-thick bismuth borate (BiBO) crystal was pumped by 4.8 fs pulses at 1 µm to generate a broadband spectrum spanning from 0.1 PHz to 0.23 PHz and 160 mW of average power. A custom-made dichroic beam splitter with the cut-off at 0.2 PHz was used to separate the residual pump from the CEP-stable pulses. After dispersion management with a custom-made CM compressor, the NIR pulses, along with the fraction of 4.8 fs pulses, were sent to a 20 µm beta barium borate (BBO) crystal for electric field sampling. The green-shaded region in Fig. 2a highlights the schematic of the NIR EOS. The up-converted signal is spectrally filtered with a pass band filter from 0.425 PHz to 0.5 PHz to enhance the detection sensitivity by eliminating the spectral components that do not carry specific field information. The measured electric field of the broadband CEP-stable pulses and its temporal intensity profile with a 15 fs pulse duration at FWHM are shown in Fig. 3a and Fig. 3b, respectively. The corresponding spectral intensity and phase obtained through the Fourier transform shown in Fig. 3c reveals residual higher-order dispersion, which can be compensated by optimizing the design of the CM compressor. While the high-frequency cut-off of the spectrum is limited by the beam splitter roll-off, the crystal absorption constrains the low-frequency cut-off to 0.1 PHz. To verify the detection sensitivity and dynamic range of the detector, the energy of the IPDFG pulses before EOS crystal was reduced from 80 nJ to subfemtojoule energies by using a series of neutral density filters. The Fig. 3a inset shows two field-resolved measurements at 8 pJ (magenta) and 0.7 fJ (in yellow), respectively. The spectral intensity counterpart at the three different pulse energies is shown in Fig. 3d corresponding to a 110 dB dynamic range. To establish the ability of the system to detect the response of minute quantities of molecules, we resolved the electric field of the atmospheric water vapour molecules, liquid water and ethanol in ambient air after excitation by femtosecond NIR pulses. The temporally gated molecular response and their frequency counterparts are shown in Fig. 4.

https://doi.org/10.1038/s41566-024-01548-2

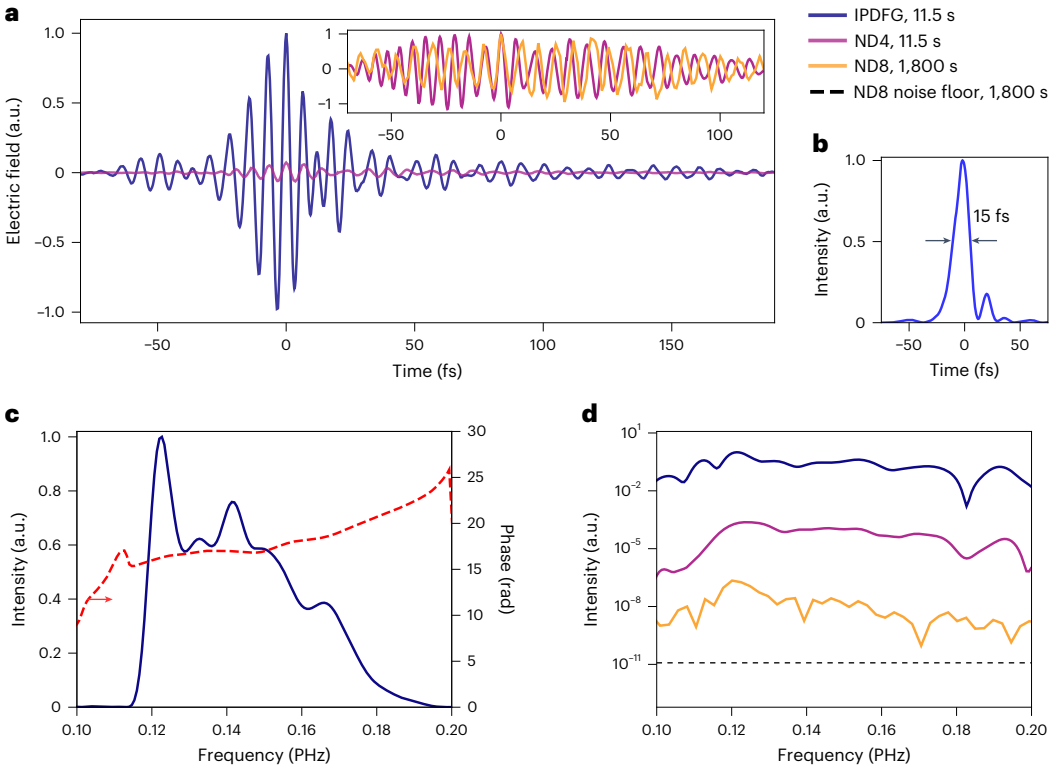

Fig. 3 | NIR electric field sampling. a, The measured electric field of CEP-stable pulses via EOS. The inset displays two low-energy fields in the presence of ND4 (magenta) and ND8 filters (yellow). Both fields are longer than the blue curve owing to additional material dispersion caused by the ND filters. **b**, The temporal profile of the CEP-stable pulses with a pulse duration of 15 fs FWHM. **c**, The retrieved spectrum and phase of the CEP-stable pulses. **d**, The retrieved spectrum of the CEP-stable pulses after attenuation with the ND4 and ND8 filters. The spectrum of the unattenuated pulse is shown in blue for comparison. The dashed black line represents the measured noise floor in the absence of the CEP-stable pulses on the balanced detector. The legend displays the acquisition time for each field, along with the ND filter label. ND, neutral density. The retrieved spectra are not corrected for the spectral response of the filters.

Discussion

Water has two prominent absorption peaks within the spectral coverage of the excitation pulses: (1) an asymmetric stretch centred at 0.115 PHz (3,836 cm^{-1}) and (2) a combination resonance of bending and asymmetrical stretch centred at 0.16 PHz (5,337 cm^{-1})[60]. Figure 4a shows the electric field of atmospheric water vapour molecules at two different laboratory relative humidities (RHs). The measurements at 50% RH and 8% RH correspond to 16.5 µmol and 2.64 µmol of atmospheric water vapour molecules interacting with the broadband 15 fs excitation pulses, respectively (Supplementary Discussion 2). The minimum laboratory-achievable RH of 8% was reached by purging the beam path with dry air and nitrogen. Figure 4b shows the corresponding absorption frequencies for both concentrations. The spectra are achieved by Fourier transformation of the temporally gated molecular response at 1 ps after the excitation pulse for a temporal window of 30 ps and agree with the HITRAN database[61] (Supplementary Fig. 4). At the 2.64 µmol level, the absorption peak at 0.16 PHz is barely resolved due to the low absorption cross-section of the water's combination band (65×10^{-21} cm^2 per molecule) compared with its counterpart at the fundamental resonance (600×10^{-21} cm^2 per molecule)[61].

Figure 4c shows the measured molecular response of 5.23 µmol and 2.64 µmol diluted water in the liquid phase, which were prepared by mixing 20 µl and 10 µl of deionized water in 1 ml acetic acid. We examined the molecular response in the liquid phase in the temporal window of 0.3 ps to 1 ps, as dephasing occurs faster (Fig. 4d)[62,63]. The absorption amplitude of both concentrations was normalized to 0.2 PHz peak, which is present at this time scale owing to the cut-off of the dichroic beam splitter used in our setup. Water's asymmetric stretch resonance at 0.115 PHz (3,836 cm^{-1}) in Fig. 4d is distinct for 5.23 µmol (red curve) and 2.64 µmol (magenta curve). The pure acetic acid response in the presence of water vapour molecules at RH of 8% is shown in Fig. 4d (black curve). To evaluate the detection sensitivity of our setup in environmental conditions, ethanol was measured due to its distinct resonance frequency in comparison with water and its low absorption cross-section. Figure 4e and Fig. 4f show the resonance of pure liquid ethanol at different concentrations and 8% RH in time and frequency domain, respectively. The weak absorption at 0.13 PHz (4,336 cm^{-1}) is due to the combination band resonance arising from the C–H stretch and C–H bend mode, which was resolved very clearly in our measurement at the minimum detectable amount of 4.13 µmol (ref. 64) (see Supplementary Fig. 5 for further analysis).

We define a figure of merit (FOM) to allow detection sensitivity comparison of absorption bands between different species and various absorption cross-sections. The FOM is defined as

$$\mathrm{FOM} = n \times \sigma, \tag{1}$$

where n is the amount of substance in mol and σ is the absorption cross-section of the absorption band in cm^2 per molecule. Given the absorption cross-section values of water (600×10^{-21} cm^2 per molecule) and ethanol (3.2×10^{-21} cm^2 per molecule)[61,65], the calculated FOM value for water at 2.64 µmol is 9×10^{-28} m^2 mol^{-1} per molecule, while FOM for ethanol's combination band at 4.13 µmol is 1.322×10^{-30} m^2 mol^{-1} per molecule with merely 25 µm path length.

In conclusion, we report on field-sensitive, near-petahertz detection of molecular fingerprints in the liquid phase. To this end, bright, intrinsically synchronized CEP-stable 15 fs pulses at 2 µm and 4.8 fs pulses at 1 µm were generated for impulsive excitation and probing of

https://doi.org/10.1038/s41566-024-01548-2

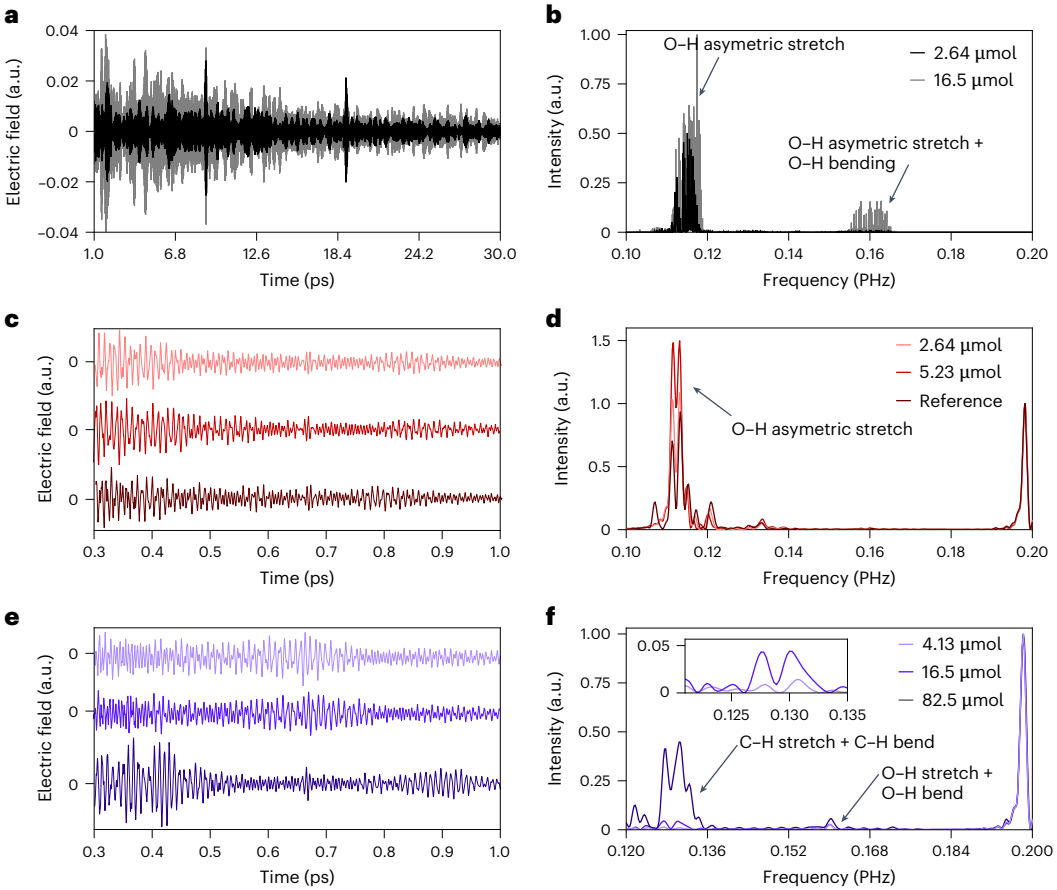

Fig. 4 | Benchmarking measurements. Each row shows the time-gated electric field on the left and its Fourier-transformed spectrum on the right. **a**, The light-grey field represents atmospheric water molecules at 50% RH (16.5 µmol), while the black curve represents 8% RH (2.64 µmol). **b**, Two absorption modes are visible: a fundamental mode at 0.115 PHz and a combination band at 0.16 PHz. **c**, Liquid water molecules at 5.23 µmol (red) and 2.64 µmol (pink) along with pure acetic acid (brown) as a reference measurement. **d**, The molecular response of pure acetic acid is compared with that of aqueous solutions. **e**, Pure liquid ethanol at different volumes of 4.13 µmol, 16.5 µmol and 82.5 µmol. **f**, The weak combination peak centred at 0.130 PHz is observed at all three volumes.

the molecular response via EOS. Using the megahertz ultrashort laser pulses, we demonstrated the ambient air field-resolved detection of femtosecond pulses with subfemtojoule energy and a 10^4 detection dynamic range in the electric field at near-petahertz frequencies[47]. The source's megahertz repetition rate augments both the signal-to-noise ratio and detection sensitivity, while the signal up-conversion in our scheme alleviates the bandwidth constraint inherent in silicon-based detectors. In a proof of concept, we reported on the sensitive detection of the vibration modes of atmospheric and aqueous water molecules at 2.64 µmol, and ethanol combination band at 4.13 µmol. These measurements mark the field-resolved detection of both fundamental and combination bands in the liquid phase.

Femtosecond pump–probe spectroscopy has provided evidence that rapid dynamics occurring within a time scale of less than 100 fs of liquid water have a significant impact on chemical reactions taking place in the aqueous phase[66]. This underscores the vital importance of ultrafast processes in comprehending aqueous phase chemistry, for example, in grasping how water molecules dissipate energy[67].The electric field measurements shown in Fig. 4 thus establish a foundation for studying aqueous solutions with enhanced sensitivity, dynamic range and attosecond temporal resolution compared with femtosecond intensity pump–probe techniques[68,69]. The enhanced detection sensitivity is rooted in the higher amplitude of the molecular response relative to the excitation pulses in field-resolved detection (Supplementary Fig. 6)[70,71]. Furthermore, the high repetition rate of near-single-cycle pulses not only lays the groundwork for single-shot monitoring of chemical reactions in liquids[72] but also presents intriguing possibilities for exploring nonlinear interactions owing to the unique combination of peak and average power in the near-single-cycle domain.

Stimulating the molecular composition of a sample with phase-coherent femtosecond excitation pulses leads to temporal gating between the molecular response from the excitation pulses. This temporal gating allows the detection of different phases of matter at weak resonance frequencies in a single measurement with high detection sensitivity, dynamic range and temporal resolution. The attosecond temporal precision of the measurements enables precise access to the subcycle electric field of light and decomposition of the short-lived liquid molecular response from the long-lived ambient gas responses (Supplementary Fig. 7). Moreover, it allows the real-time resolution of both molecular and electronic dynamics within matter[73–76]. Employing probe pulses with shorter temporal duration extends the detection bandwidth of EOS up to visible frequencies, constrained by the absorption of the gate pulses in ambient air. The high repetition rate of the source enables tracking the sample's dynamic temporal evolution on a time scale of hundreds of milliseconds. Capturing spectrograms with exceptional temporal and spectral resolution offers information akin to that of multidimensional spectroscopy, yet with a more straightforward and sturdy setup. This is particularly beneficial for liquid samples that feature broad bandwidths and intricate spectral resonances. Femtosecond fieldoscopy expands the scope of aqueous sample analysis and paves the path towards novel methods

for multidimensional spectroscopy and high-resolution biological spectro-microscopy[77–80].

Online content

Any methods, additional references, Nature Portfolio reporting summaries, source data, extended data, supplementary information, acknowledgements, peer review information; details of author contributions and competing interests; and statements of data and code availability are available at https://doi.org/10.1038/s41566-024-01548-2.

References

1. Han, L. et al. Understanding the water structures by near-infrared and Raman spectroscopy. *J. Raman Spectrosc.* **53**, 1686–1693 (2022).
2. Blanco, M. & Villarroya, I. NIR spectroscopy: a rapid-response analytical tool. *Trends Anal. Chem.* **21**, 240–250 (2002).
3. Espinoza, L. H., Lucas, D. & Littlejohn, D. Characterization of hazardous aqueous samples by near-IR spectroscopy. *Appl. Spectrosc.* **53**, 97–102 (1999).
4. Marx, V. It's free imaging—label-free, that is. *Nat. Methods* **16**, 1209–1212 (2019).
5. Gowen, A. et al. On the feasibility of near infrared spectroscopy to detect contaminants in water using single salt solutions as model systems. *Talanta* **131**, 609–618 (2015).
6. Fiddler, M. N. et al. Laser spectroscopy for atmospheric and environmental sensing. *Sensors* **9**, 10447–10512 (2009).
7. Martin, P. A. Near-infrared diode laser spectroscopy in chemical process and environmental air monitoring. *Chem. Soc. Rev.* **31**, 201–210 (2002).
8. Li-Chan, E., Chalmers, J. M. & Griffiths, P. R. *Applications of Vibrational Spectroscopy in Food Science, 2 Volume Set* (John Wiley & Sons, 2010).
9. Leighton, R. E., Alperstein, A. M. & Frontiera, R. R. Label-free super-resolution imaging techniques. *Annu. Rev. Anal. Chem.* **15**, 37–55 (2022).
10. Krafft, C. et al. Label-free molecular imaging of biological cells and tissues by linear and nonlinear Raman spectroscopic approaches. *Angew. Chem. Int. Ed.* **56**, 4392–4430 (2017).
11. Haas, J. & Mizaikoff, B. Advances in mid-infrared spectroscopy for chemical analysis. *Annu. Rev. Anal. Chem.* **9**, 45–68 (2016).
12. Burns, D. A. & Ciurczak, E. W. *Handbook of Near-Infrared Analysis* (CRC Press, 2007).
13. Beć, K. B. & Huck, C. W. Breakthrough potential in near-infrared spectroscopy: spectra simulation. a review of recent developments. *Front. Chem.* **7**, 48 (2019).
14. Türker-Kaya, S. & Huck, C. W. A review of mid-infrared and near-infrared imaging: principles, concepts and applications in plant tissue analysis. *Molecules* **22**, 168 (2017).
15. Kuda-Malwathumullage, C. P. & Small, G. W. Determination of temperatures of aqueous-based samples directly from near infrared spectra. *J. Near Infrared Spectrosc.* **25**, 289–300 (2017).
16. Beć, K. B., Grabska, J. & Huck, C. W. Near-infrared spectroscopy in bio-applications. *Molecules* **25**, 2948 (2020).
17. McClure, W. F. 204 years of near infrared technology: 1800–2003. *J. Near Infrared Spectrosc.* **11**, 487–518 (2003).
18. Pasquini, C. Near infrared spectroscopy: a mature analytical technique with new perspectives—a review. *Anal. Chim. Acta* **1026**, 8–36 (2018).
19. Whetsel, K. B. Near-infrared spectrophotometry. *Appl. Spectrosc. Rev.* **2**, 1–67 (1968).
20. Zolot, A. M. et al. Broad-band frequency references in the near-infrared: accurate dual comb spectroscopy of methane and acetylene. *J. Quant. Spectrosc. Radiat. Transfer* **118**, 26–39 (2013).
21. Zhu, F. et al. Real-time dual frequency comb spectroscopy in the near infrared. *Appl. Phys. Lett.* **102**, 121116 (2013).
22. Iwakuni, K. et al. Ortho-para-dependent pressure effects observed in the near infrared band of acetylene by dual-comb spectroscopy. *Phys. Rev. Lett.* **117**, 143902 (2016).
23. Coddington, I., Newbury, N. & Swann, W. Dual-comb spectroscopy. *Optica* **3**, 414–426 (2016).
24. Barreiro, R., Sanabria-Macías, F., Posada, J., Martín-Mateos, P. & de Dios, C. Experimental demonstration of a new near-infrared spectroscopy technique based on optical dual-comb: DC-NIRS. *Sci. Rep.* **13**, 10924 (2023).
25. Andrews, N. L. et al. Quantification of different water species in acetone using a NIR-triple-wavelength fiber laser. *Opt. Express* **22**, 19337–19347 (2014).
26. Sommer, A. et al. Attosecond nonlinear polarization and light–matter energy transfer in solids. *Nature* **534**, 86–90 (2016).
27. Riek, C. et al. Direct sampling of electric-field vacuum fluctuations. *Science* **350**, 420–423 (2015).
28. Itatani, J. et al. Attosecond streak camera. *Phys. Rev. Lett.* **88**, 173903 (2002).
29. Goulielmakis, E. et al. Direct measurement of light waves. *Science* **305**, 1267–1269 (2004).
30. Keiber, S. et al. Electro-optic sampling of near-infrared waveforms. *Nat. Photonics* **10**, 159–162 (2016).
31. Cho, W. et al. Temporal characterization of femtosecond laser pulses using tunneling ionization in the UV, visible, and mid-IR ranges. *Sci. Rep.* **9**, 16067 (2019).
32. Park, S. B. et al. Direct sampling of a light wave in air. *Optica* **5**, 402–408 (2018).
33. Saito, N., Ishii, N., Kanai, T. & Itatani, J. All-optical characterization of the two-dimensional waveform and the Gouy phase of an infrared pulse based on plasma fluorescence of gas. *Opt. Express* **26**, 24591–24601 (2018).
34. Alismail, A. et al. Multi-octave, CEP-stable source for high-energy field synthesis. *Sci. Adv.* **6**, eaax3408 (2020).
35. Korobenko, A. et al. Femtosecond streaking in ambient air. *Optica* **7**, 1372–1376 (2020).
36. Sederberg, S. et al. Attosecond optoelectronic field measurement in solids. *Nat. Commun.* **11**, 430 (2020).
37. Sulzer, P. et al. Determination of the electric field and its Hilbert transform in femtosecond electro-optic sampling. *Phys. Rev. A* **101**, 033821 (2020).
38. Zimin, D. et al. Petahertz-scale nonlinear photoconductive sampling in air. *Optica* **8**, 586–590 (2021).
39. Liu, Y. et al. All-optical sampling of few-cycle infrared pulses using tunneling in a solid. *Photonics Res.* **9**, 929–936 (2021).
40. Hui, D. et al. Attosecond electron motion control in dielectric. *Nat. Photonics* **16**, 33–37 (2022).
41. Zimin, D. A., Yakovlev, V. S. & Karpowicz, N. Ultra-broadband all-optical sampling of optical waveforms. *Sci. Adv.* **8**, eade1029 (2022).
42. Ridente, E. et al. Electro-optic characterization of synthesized infrared-visible light fields. *Nat. Commun.* **13**, 1111 (2022).
43. Altwaijry, N. et al. Broadband photoconductive sampling in gallium phosphide. *Adv. Opt. Mater.* **11**, 2202994 (2023).
44. Luo, Y., Martin-Jimenez, A., Neubrech, F., Liu, N. & Garg, M. Synthesis and direct sampling of single-cycle light transients by electron tunneling in a nanodevice. *ACS Photonics* **10**, 2866–2873 (2023).
45. Kempf, H., Sulzer, P., Liehl, A., Leitenstorfer, A. & Tenne, R. Few-femtosecond phase-sensitive detection of infrared electric fields with a third-order nonlinearity. *Commun. Phys.* **6**, 145 (2023).
46. Yeung, M. et al. Lightwave electronic harmonic frequency mixing. *Sci. Adv.* **10**, eadq0642 (2024).
47. Herbst, A. et al. Recent advances in petahertz electric field sampling. *J. Phys. B* **5**, 172001 (2022).
48. Mamaikin, M., Ridente, E., Altwaijry, N., Weidman, M. & Karpowicz, N. Contrast enhancement in near-infrared electro-optic imaging. *Opt. Express* **30**, 18179–18188 (2022).

49. Barh, A., Rodrigo, P. J., Meng, L., Pedersen, C. & Tidemand-Lichtenberg, P. Parametric upconversion imaging and its applications. *Adv. Opt. Photonics* **11**, 952–1019 (2019).
50. Okamoto, T. et al. Operation at 1 MHz of 1.7-cycle multiple plate compression at 35-W average output power. *Opt. Lett.* **48**, 2579–2582 (2023).
51. Goncharov, S., Fritsch, K. & Pronin, O. Few-cycle pulse compression and white light generation in cascaded multipass cells. *Opt. Lett.* **48**, 147–150 (2023).
52. Baltuška, A., Wei, Z., Pshenichnikov, M. S. & Wiersma, D. A. Optical pulse compression to 5 fs at a 1-MHz repetition rate. *Opt. Lett.* **22**, 102–104 (1997).
53. Köttig, F., Schade, D., Koehler, J., Russell, P. S. J. & Tani, F. Efficient single-cycle pulse compression of an ytterbium fiber laser at 10 MHz repetition rate. *Opt. Express* **28**, 9099–9110 (2020).
54. Porer, M., Ménard, J.-M. & Huber, R. Shot noise reduced terahertz detection via spectrally postfiltered electro-optic sampling. *Opt. Lett.* **39**, 2435–2438 (2014).
55. Travers, J. C., Chang, W., Nold, J., Joly, N. Y. & Russell, P. S. J. Ultrafast nonlinear optics in gas-filled hollow-core photonic crystal fibers. *JOSA B* **28**, A11–A26 (2011).
56. Russell, P. S. J., Hölzer, P., Chang, W., Abdolvand, A. & Travers, J. Hollow-core photonic crystal fibres for gas-based nonlinear optics. *Nat. Photonics* **8**, 278–286 (2014).
57. Schade, D. et al. Scaling rules for high quality soliton self-compression in hollow-core fibers. *Opt. Express* **29**, 19147–19158 (2021).
58. Koehler, J., Köttig, F., Schade, D., Russell, P. S. J. & Tani, F. Post-recombination effects in confined gases photoionized at megahertz repetition rates. *Opt. Express* **29**, 4842–4857 (2021).
59. Fattahi, H., Schwarz, A., Keiber, S. & Karpowicz, N. Efficient, octave-spanning difference-frequency generation using few-cycle pulses in simple collinear geometry. *Opt. Lett.* **38**, 4216–4219 (2013).
60. Levine, I. N. *Molecular Spectroscopy* (Wiley, 1975).
61. Gordon, I. et al. The HITRAN2020 molecular spectroscopic database. *J. Quant. Spectrosc. Radiat. Transfer* **277**, 107949 (2022).
62. Falk, M. The frequency of the hoh bending fundamental in solids and liquids. *Spectrochim. Acta Part A* **40**, 43–48 (1984).
63. Bruenig, F. N., Geburtig, O., Canal, A. V., Kappler, J. & Netz, R. R. Time-dependent friction effects on vibrational infrared frequencies and line shapes of liquid water. *J. Phys. Chem. B* **126**, 1579–1589 (2022).
64. Davies, A. & Rutland, S. G. Identification of an OH, CH combination band in the near infrared spectrum of ethanol. *Spectrochim. Acta Part A* **44**, 1143–1145 (1988).
65. Sharpe, S. W. et al. Gas-phase databases for quantitative infrared spectroscopy. *Appl. Spectrosc.* **58**, 1452–1461 (2004).
66. Jimenez, R., Fleming, G. R., Kumar, P. & Maroncelli, M. Femtosecond solvation dynamics of water. *Nature* **369**, 471–473 (1994).
67. Perakis, F. et al. Vibrational spectroscopy and dynamics of water. *Chem. Rev.* **116**, 7590–7607 (2016).
68. Maiuri, M., Garavelli, M. & Cerullo, G. Ultrafast spectroscopy: state of the art and open challenges. *J. Am. Chem. Soc.* **142**, 3–15 (2014).
69. Crowell, R. A., Holtom, G. R. & Xie, X. S. Infrared free induction decay of liquid water molecules. *J. Phys. Chem.* **99**, 1840–1842 (1995).
70. Pupeza, I. et al. Field-resolved infrared spectroscopy of biological systems. *Nature* **577**, 52–59 (2020).
71. Kowligy, A. S. et al. Infrared electric field sampled frequency comb spectroscopy. *Sci. Adv.* **5**, eaaw8794 (2019).
72. Couture, N. et al. Single-pulse terahertz spectroscopy monitoring sub-millisecond time dynamics at a rate of 50 kHz. *Nat. Commun.* **14**, 2595 (2023).
73. Kienberger, R. et al. Atomic transient recorder. *Nature* **427**, 817–821 (2004).
74. Alqattan, H., Hui, D., Sennary, M. & Hassan, M. T. Attosecond electronic delay response in dielectric materials. *Faraday Discuss.* **237**, 317–326 (2022).
75. Scheffter, K. et al. Compressed sensing of field-resolved molecular fingerprints beyond the Nyquist frequency. *Ultrafast Sci.* **4**, 0062 (2024).
76. Oliver, T. A. A. Recent advances in multidimensional ultrafast spectroscopy. *R. Soc. Open Sci.* **5**, 171425 (2018).
77. Fattahi, H. Method and apparatus for creating a microscopic sample image of a molecular vibrational response of a sample. US patent app. 18/024,120 (2023).
78. Mukamel, S., Tanimura, Y. & Hamm, P. Coherent multidimensional optical spectroscopy. *Acc. Chem. Res.* **42**, 1207–1209 (2009).
79. Jun, S. et al. Nonlinear dynamics of femtosecond laser interaction with the central nervous system in zebrafish. *Commun. Phys.* **7**, 161 (2024).
80. Abramavicius, D., Palmieri, B., Voronine, D. V., Sanda, F. & Mukamel, S. Coherent multidimensional optical spectroscopy of excitons in molecular aggregates; quasiparticle versus supermolecule perspectives. *Chem. Rev.* **109**, 2350–2408 (2009).

Method

Near-single-cycle pulse generation

A commercially available Yb:KGW amplifier (CARBIDE Light Conversion) delivering 255 fs pulses at 1,030 nm with 20 W of average power and at 1 MHz repetition rate is used as the source laser. In the first nonlinear fibre stage, we used a 100 mm focal length (Thorlabs LA1509-B-ML) lens to couple 20 µJ circularly polarized pulses into a 50-cm-long SR-PCF with a core diameter of 55 µm (Supplementary Fig. 8) filled with 15 bar of argon. The spectrally broadened laser pulses were compressed to 25 fs (FWHM) using a CM compressor (UltraFast Innovations GmBH PC1611) with 16 bounces (Supplementary Fig. 9). The total group delay dispersion compensated by the CM compressor was −2,400 fs^2. Subsequently, the 25 fs compressed pulses were coupled (via Thorlabs LA1509-BML) to a 31-cm-long SR-PCF (parameter same as before), filled with 15 bar of helium. After the second stage, a 2-inch off-axis silver parabola (Edmund 36-598) with an effective focal length of 177.8 mm was used to collimate the beam. The two gas cells were mounted on a three-axis stage (MDE122) from Elliot Scientific. The two-stage fibre system achieves a total throughput of 85% before the collimating parabola. Afterwards, the soliton-compressed pulses were sent to a CM compressor (UFI PC105) consisting of four double-angle CM (total group delay dispersion of −160 fs^2) and a pair of wedges (Altechna M0067705) to compensate for the dispersion caused by the 2-mm-thick MgF_2 output window of the second gas cell and to pre-compensate for the accumulated dispersion on the pulse before reaching the IPDFG crystal. After the compressor, we placed a 1 mm anti-reflective (AR)-coated window (UFI AR7203) that reflects 5% of the beam, to separate the probe pulses for EOS. We employed a home-built second-harmonic generation frequency-resolved optical gating (SHG-FROG) for temporal characterization. To ensure accurate measurements, the device utilized all-reflective dispersion-free optics in a non-collinear geometry with 20-µm-thick BBO crystal (Castech) cut for type I phase matching.

CEP-stable NIR pulse generation

For the IPDFG, we focused 12 µJ of the compressed pulses from the fibre stages to 40 µm by using a 1-inch off-axis parabola. A type I BiBO crystal with a phase matching angle of 11° (Castech) was placed a few millimetres behind the focus to avoid white light generation in the crystal. A half-wave plate was introduced into the beam path before the second fibre stage to project 14% of the input pulses to the fast axis of the crystal. The generated CEP-stable pulse was collimated to a beam size of 3.2 mm at 1 e^{-2} employing a 4-inch focal length parabola (Thorlabs MPD254508-90-P01). A custom-built (UFI BS2214-RC2) broadband dichroic beam splitter separated the pump and the NIR beam. The measured power after the beam splitter was 160 mW. A custom-built double-angle CM compressor (UFI IR7202) (Supplementary Fig. 10) with four bounces was used for temporal compression to 15 fs.

Field-resolved detection

In EOS, probe and excitation pulses propagate collinearly in a nonlinear crystal, generating spectral components at sum and difference frequencies. The up-converted field-sensitive signal arises from the interference between partially overlapping spectra of the probe pulse and the sum or difference frequency pulse. Through an ellipsometer, direct access is obtained to the electric field of the sampled pulse[37]. By utilizing a lock-in amplifier and balanced detection, the technical noise surplus of the gate pulse was mitigated, thereby making the shot noise of the probe pulse the primary limitation on detection sensitivity. In the EOS, the IPDFG pulses were used as an excitation pulse, whereas a 5% reflection from the second fibre stage's output was used as a probe pulse. A wire grid polarizer combined the probe and the excitation pulses with orthogonal polarization, collinearly in the EOS crystal. An off-axis parabolic mirror of 3-inch focal length was used to focus the beams in a 20-µm-thick type II BBO crystal to generate the sum frequency signal. The sum frequency signal interferes with the high-frequency portion of the probe pulse, which acts as a local oscillator for heterodyne detection. Appropriate filters (Thorlabs FEL 600 and FES 700) were placed after the EOS crystal. The resulting polarization rotation was measured by an ellipsometer, which included a Wollaston prism, a quarter-wave plate and balanced photodiodes. The quarter-wave plate is adjusted to ensure that both photodiodes receive the same intensity in the presence of the probe pulses. A mechanical chopper modulated the excitation pulses at 5.8 kHz to enable heterodyne lock-in detection. The delay line was based on the linear motorized stage (Physik Instrument V-528.1AA) with a scanning range of 20 mm, corresponding to a scanning delay of 132 ps. An interferometric delay tracking system[81] was employed to precisely track the delay line and any timing jitter artefacts (Supplementary Information).

In EOS, the measured interference of the sampling field with sum frequency field components is convoluted with the detector response. Consequently, it is subject to a complex response function comprising both amplitude and phase components. The response function can be calculated using the methods described in ref. 30. Based on the wavevector mismatch calculation (Supplementary Fig. 11), it can be seen that the post-processing of the measured field can be neglected for our spectral range as the nonlinear response remains constant throughout the EOS detection range.

Sample preparation

A Pike Technologies liquid cell (162–1,200) with two 3-mm-thick barium fluoride windows and a spacer was used to hold the liquid samples. To examine the liquid water, 10 µl and 20 µl of deionized water were mixed with 1 ml acetic acid buffer solution (chemlab, CL00.0119). The samples were placed between two windows using a 0.5 mm Teflon O-ring, corresponding to an irradiation volume of 4.81 µl. Three cells with different concentrations were mounted side by side on a translation stage to reduce the systematic error. For ethanol measurements, pure ethanol (VWR Chemicals, 85033.360) was filled into three liquid cells with Teflon O-ring spacers of different thicknesses (0.5 mm, 0.1 mm and 0.025 mm). The spacers corresponded to irradiation volumes of 4.81 µl, 0.962 µl and 0.241 µl, respectively.

Data availability

The data may be obtained from the corresponding author upon reasonable request.

Code availability

All relevant code is available from the corresponding authors upon reasonable request.

References

81. Schweinberger, W. et al. Interferometric delay tracking for low-noise Mach–Zehnder-type scanning measurements. *Opt. Express* **27**, 4789–4798 (2019).

Acknowledgements

This work was supported by research funding from the Max Planck Society. We thank P. S. J. Russell, M. H. Frosz and their team for the production of the fibres used in this experiment. We thank D. Schade, W. Schweinberger, G. Arisholm, N. Karpowicz and M. I. Suresh for their invaluable support.

Author contributions

H.F. envisioned and designed the experiment. A.S., A.H., F.T. and M.K. implemented fibre stages for short pulse generation. A.S., A.H. and M.M.B. implemented the data acquisition system. A.S. performed the fieldoscopy measurements. A.S. and H.F. performed the data analysis and wrote the manuscript. All authors proofread the manuscript.

Funding
Open access funding provided by Max Planck Society.

Competing interests
The authors do not declare any competing interests.

Additional information
Supplementary information The online version contains supplementary material available at https://doi.org/10.1038/s41566-024-01548-2.

Correspondence and requests for materials should be addressed to Hanieh Fattahi.

Peer review information *Nature Photonics* thanks Mohammed Hassan and the other, anonymous, reviewer(s) for their contribution to the peer review of this work.